BOR DERGİSİ
JOURNAL OF BORON
http://dergipark.org.tr/boron

Investigation of the structural and magnetic properties of $Fe_{70}Ti_{10}B_{20}$ (at.%) alloys by mechanical alloying

Tuncay Şimşek*

Mersin University, Department of Industrial Design, 33343 Mersin, Turkey, ORCID ID orcid.org/ 0000-0002-4683-0152

ARTICLE INFO

Article history:
Received 21 December 2018
Revised form 29 May 2019
Accepted 09 June 2019
Online 30 June 2019

Research Article

DOI: 10.30728/boron.500470

Keywords:
Mechanical alloying,
Nanoparticles,
Magnetic properties,
Amorphous alloys

ABSTRACT

In this study, amorphous/nanocrystalline $Fe_{70}Ti_{10}B_{20}$ (at.%) alloys were synthesized by using elemental Fe, Ti and B powders under argon gas atmosphere via mechanical alloying method. The powders were ball milled at 20:1 ball to powder ratio and 500 rpm rotating speed up to 70 h. The phase and morphological properties of the synthesized powders were examined by using X-Ray diffractometer and scanning electron microscopy with energy-dispersive X-ray spectroscopy (SEM/EDX). The magnetic properties of powders were determined by vibrating sample magnetometer (VSM) at room temperature in the range of 0-20 kOe. It is determined that after 2.5 h of milling Ti and B are started to dissolve in Fe lattice and Fe(TiB) solid solutions formed. XRD analysis revealed that the amorphous structures were formed after 30 h of milling and the crystallite size and lattice strain were found around 8.2 nm and %1.16, respectively. SEM images indicated that the particles were mostly agglomerated and the particles size distribution was in the range of 10-48 µm. Magnetic measurements revealed that after 70 h of milling, the saturation magnetization (M_s) and the coercivity (H_c) reached about 94 emu/g and 117 Oe.

1. Introduction

Mechanical alloying (MA) is an intensively used solid-state material synthesis method that provides a wide range of stable and metastable materials such as intermetallic, supersaturated solid solution, nanocrystalline and amorphous alloys [1-3]. The MA is mostly preferred due to its simplicity, relatively low-cost equipment, flexibility of the processes and ability to allow material synthesis such as equilibrium and non-equilibrium materials at room temperature. During the mechanisms such as continuous flattening, cold welding and re-breaking of particles various nanostructured materials and amorphous particles can be synthesized in the range of several microns to nanometer scales [1-5]. Especially, some features of synthesized nanostructured materials such as high strength, hardness, ductilization of brittle materials and enhanced diffusivity have superior properties compared to traditional materials [6-8].

The advances in material technology and the increase in application areas have further increased the interest in magnetic materials. Among the magnetic materials, many studies have been carried out in particular about Fe-based magnetic materials. Fe-based amorphous/nanocrystalline alloys have a wide application area due to their good soft magnetic properties, corrosion resistance and also relatively low casting properties [9-13]. The usage of iron-based alloys can be seen in applications such as sensor probes, solenoid end caps and switches, transformer magnets, magnetic cores, information storage, and in high-frequency electronic devices [9,14-16]. In the literature, it is seen that various amorphous/nanocrystalline Fe alloys have been produced successfully by the mechanochemical method. In recent years, Baghbaderani et al., investigated the nanostructure formation and magnetic properties of $Fe_{45}Co_{45}Ni_{10}$ alloys with elemental Fe, Co and Ni powders by high energy ball milling and reported that after 20-35 h of milling the $Fe_{45}Co_{45}Ni_{10}$ alloys with 10 nm grain size and 186 emu/g magnetization saturation was obtained [17]. In study of Yousefi et al., the nanocrystalline Fe(Co) and Fe(Co,Si) solid solution was synthesized with Fe-Co-Si powders by mechanochemical method [18]. In study by Younes et al., the structural and magnetic properties of FeCuNi nanostructures were investigated and they reported that the crystallite size was decreased with Ni content while coercivity and saturation magnetization increases by the increase of the Cu concentration [19]. In another study performed by Alleg et al., the magnetic and structural characterization of the mechanically alloyed $Fe_{75}Si_{15}B_{10}$ powders were determined. They indicated that the dissolution of B and Si into the Fe lattice leads to the formation of bcc α-Fe(Si,B) solid solution, the coercivity and magnetization values were found as 55 Oe and 6.7 emu/g, respectively, after 150 h of milling. [20]. Ipus et al., studied the magnetic properties of FeNbB alloy by using crystalline and amorphous boron during MA. Their results pointed out that particularly for short milling times, amorphous boron was more

*Corresponding author: tuncaysimsek@mersin.edu.tr

efficiently incorporated into the matrix than crystalline one [21]. In another study, Okumara et al., studied the mechanical alloying of Fe-B alloys. They reported in their work that the amorphous phase can be successfully obtained with composition of $Fe_{70}B_{30}$ and they also indicated that using higher boron concentration, increases excessively the milling time for the formation of iron and boron compounds [22]. Furthermore in some studies the effects of metalloids contents to the glass-forming ability in Fe-based alloys systems were reported [23,24]. Lu et al., [25] and Shen et al., [26] claimed that at least 20 at.% metalloid content such as B, C, Si, and P or even more in Fe-based alloy systems remarkably enhanced glass-forming ability.

The aim of the present study is to investigate the structural and magnetic properties of $Fe_{70}Ti_{10}B_{20}$ (at.%) alloys by mechanical using elemental crystalline Fe, Ti and B powders. B and Ti was added to the iron-based alloy systems due to their amorphous phase formation and glass-forming ability [27,28]. The evolution of phase and morphological structures were characterized by using X-Ray diffractometer and scanning electron microscopy. Magnetic properties were determined by using vibrating sample magnotometer at room temperature in the range of 0-20 kOe

2. Materials and methods

In this study, the elemental powders of iron (Riedel-de Haen, < 212 μm, 99%), titanium (Aldrich, < 150 μm, 99.7%) and amorphous boron (Alfa Easer, < 45 μm, 99%) used as initial powders. The initial powders were weighted in the argon filled glove-box using high precision balance to give a nominal composition of $Fe_{70}Ti_{10}B_{20}$ (at.%). MA experiments were performed with planetary type ball mill (Retch, PM 100 CM, monomill) under Ar gas atmosphere. The hardened steel vial and balls were used and ball to powder ratio was selected as 20:1. In the MA experiments, the rotation speed was fixed to 500 rpm and total weight of powder mixtures was about 30 g. To increase the efficiency and also to avoid excessive heating during milling, after each 30 minutes of milling, instrument was paused for 15 min and every 45 minutes' rotational direction was changed to clockwise/counter-clockwise. The milling was prolonged to 70 h and at preselected times (2.5, 5, 10, 20, 30, 40, 50, 60, 70) the powders were unloaded again in the glove-box and small amount of powders were taken from vial for characterization. The mean crystallite size and lattice strain were calculated by using the Williamson-Hall method (1) [29];

$$B\cos\theta = \frac{(K\lambda)}{D} + \varepsilon sin\,\theta \qquad (1)$$

where B is the full-width at half-maximum of the diffraction peak, θ is the Bragg angle, K is a constant whose value is 0.9, ε is the internal microstrain, λ is the wavelength of the X-ray and D is the crystallite size. The phase structures and amorphous phase formation of as-alloyed powders were analyzed by X-Ray diffractometer (Panalytical Empyrean) with CuKα radiation (λ=1.54Å) at 45V anode voltage and 40 mA current, from 2θ=10º to 90º and 4º/min scanning rate. Morphological and microstructural investigation was investigated by using SEM/EDX with a FEI-Quanta FEG 450 microscope operated at 12.3 kV in secondary electron mode. Furthermore, the particle size distribution was determined by ImageJ Analyzer software. Magnetic properties of $Fe_{70}Ti_{10}B_{20}$ (at.%) alloys were investigated at room temperature by using the vibrating sample magnetometer (VSM) under a magnetic field of ± 20 kOe.

3. Results and discussion

The powder mixture of elemental Fe, Ti and B were ball milled at different milling times and the phase transformations of powders mixture was investigated by XRD. The XRD graphs of initial powders up to 70 h of milling periods are given in Figure 1. As seen from Figure 1, the reflected peaks of crystalline Fe (ICDD

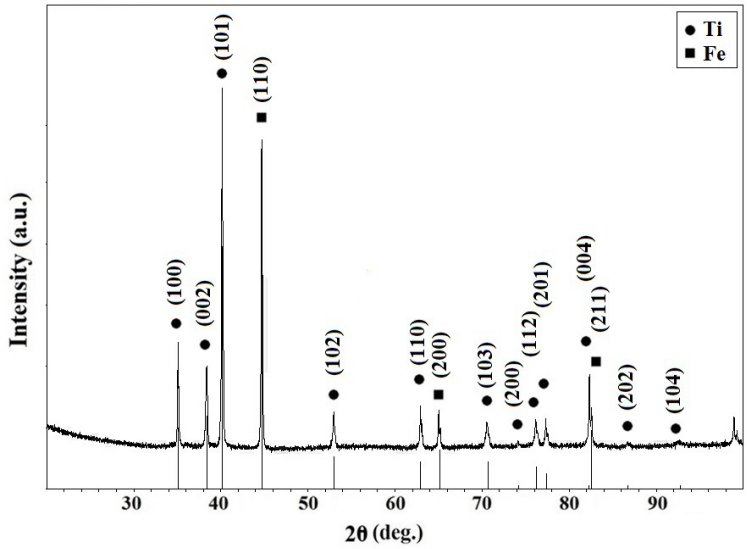

Figure 1. XRD graphs of initial powders

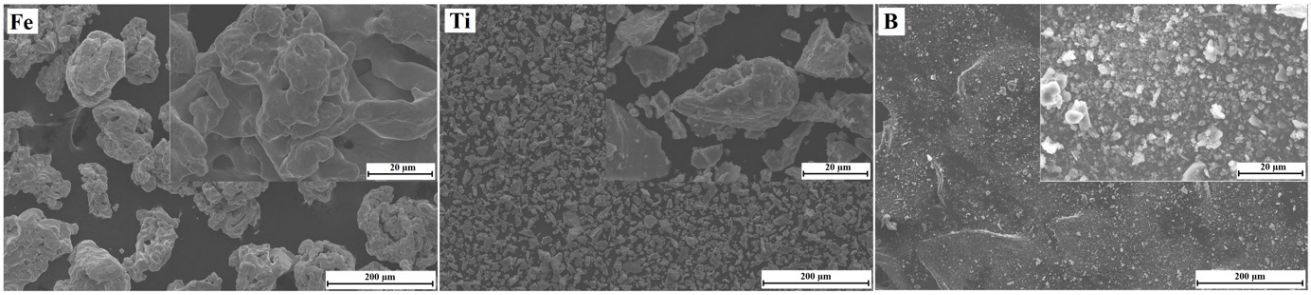

Figure 2. SEM image of initial materials.

Card No: 87-0722, cubic, *Im-3m)* and Ti (ICDD Card No: 44-1294, hexagonal, *P63/mmc*) were seen while the peaks of B were not seen because of its low atomic scattering factor and amorphous structure.

The morphological structure of the initial powders is given in Figure 2. The irregular/coaxial shaped of Fe and flat/irregular form of Ti and B were observed. It is noticed that most of the powders were agglomerated and particle size distribution of Fe, Ti and B powders were in the range of 5-200, 1-50 and 1-10 µm, respectively.

Figure 3 presents the structural evolution of the mechanical alloyed powders for different milling periods by XRD analysis. It is seen that at the end of the 2.5 h milling, the intensity of elemental peaks decreased rapidly and some of them disappeared. As the milling continues, the peak observed at around 2θ=44.74 was continued to expand up to 30 h milling and the peak height decreased and the area beneath decreased. These changes were ascribed to decrease in grain size and increase in the lattices strain [30,31]. The disappearance of the Ti peaks after 2.5 h of milling indicates that Ti began to dissolve in Fe lattice and solid solution of Fe(TiB) formed. The similar results were observed in the studies of Karimi et al. They reported that during ball milling of $Ni_{63}Fe_{13}Mo_4Nb_{20}$ alloy, as milling time increases formation of the Ni (Fe, Nb, Mo) solid solution was achieved due to the complete diffusion of Fe, Nb and Mo into the Ni lattice [32]. After 30 h of milling the all crystalline peaks nearly disappeared and the single broad peak continued to expand up to 70 h milling. It is noticed that during synthesis of the ternary Fe, Ti and B elements via MA, firstly the Fe(TiB) solid solution was obtained and then the amorphous phases of Fe(TiB) were formed.

The mean crystallite size and micro-strain were calculated from the Fe (2θ=44.74) reflection peaks according to Williamson-Hall method. Figure 4a exhibits the variation of crystallite size as a function of the milling time. It is clearly seen that the crystallite size was rapidly decreased during the first 10 h milling and continues to decrease with increasing milling time. The crystallite size was calculated as 32.35 nm for 2.5 h of milling and it decreased to 8.2 nm after 30 h of milling. Figure 4b exhibits the time dependence of the lattice strain. It is noticed that the lattice strain was increased on continuous milling periods and calculated about 1.1% at 30 h of milling. The increases in lattice strain was attributed the increase in grain

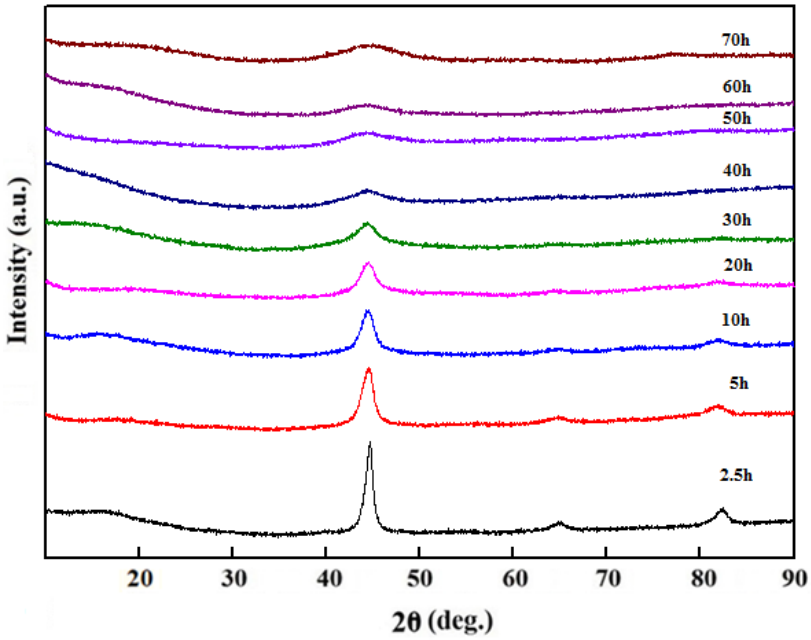

Figure 3. XRD pattern of ball milled $Fe_{70}Ti_{10}B_{20}$ (at.%) powders

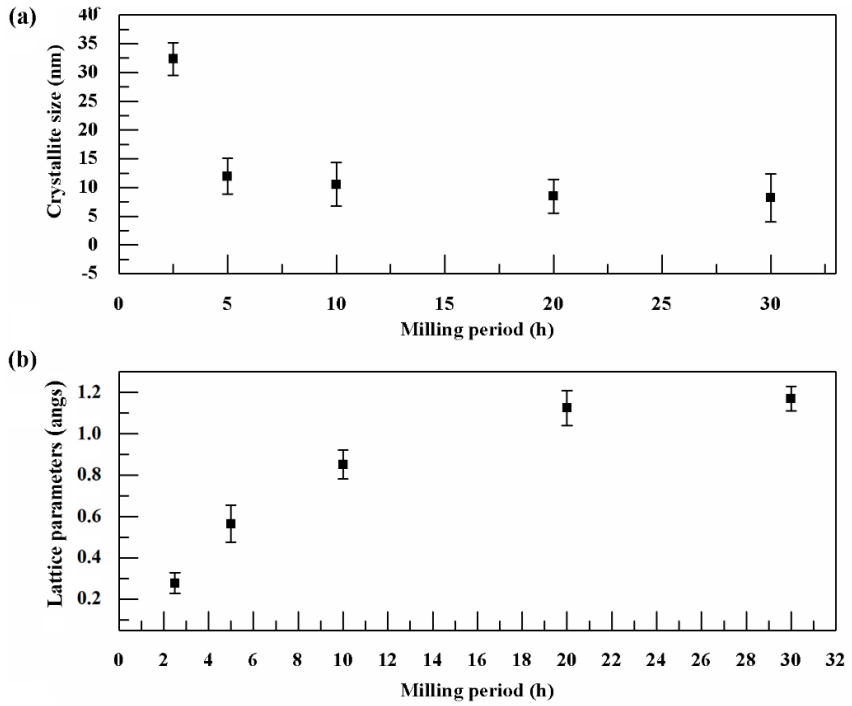

Figure 4. (a) Crystallite size and (b) Lattice strain dependency to milling period.

boundaries fraction ratios and the dislocation intensity due to the heavy plastic deformation. Generally, the micro-strains in the mechanical alloyed powders are caused by the various crystal defects such as vacancies, dislocations, shear planes, thermal expansions and contractions and increases with deformation of powders during milling processes [1,33,34]. This situation was frequently encountered in MA processes. As expected, during the longer milling period, repeated cold welding, flattening and fracture lead to increase in the energy of the particles and caused to decrease in crystallite size while increase in the lattice strain was observed. The results obtained are in good agreement with the literature [11-19,20,30-31].

As it is well known, several mechanisms occurs during

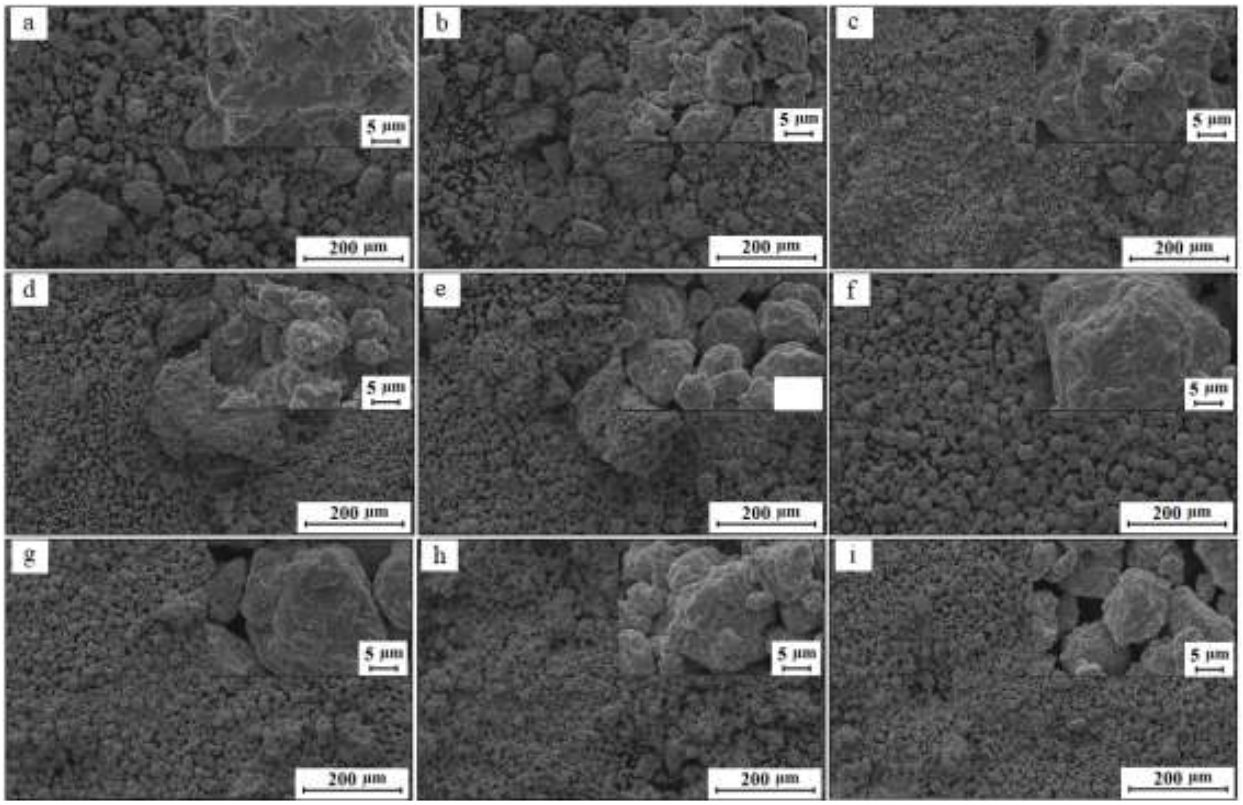

Figure 5. SEM graphs of mechanical alloyed $Fe_{70}Ti_{10}B_{20}$ (at.%) powder for different milling period (h) a) 2.5, b) 5, c) 10, d) 20, e)30, f) 40, g) 50, h) 60, i) 70.

the MA processes. The particles subject to intensive collision of balls and vials. As a result of the impact energy generated by the balls in the vial, the particles are flattening, welded, broken and re-welded. When the ductile and brittle materials are milled together, the brittle powders are separated into smaller pieces and trapped inside the ductile powders [1]. In the milling of $Fe_{70}Ti_{10}B_{20}$ (at.%) alloy, the Fe element acts as ductile material and absorbs the elemental powders Ti and B in the initial phase of the milling process [31]. As can be seen from the SEM image given in Figure 5, at the beginning of the milling process (0-30 h) as a result of the reactions between elemental powders by deformation, the alloyed powders are continuously welded, broken and have been agglomerated to the larger powders. It was seen that these sequential welding of the little particles on to the surface of larger ones increased the particles size during milling [9]. However, with increasing milling time (40-70 h), particles that reach a certain size have started to break down due to the energy generated by the impact of the milling balls. The breakdown of hardened ductile powders also led to homogenization of the Ti and B metals in the metal matrix. In the final phase of the MA process, the particles were re-broken again with the continuous deformation and subsequently the structure of the particles became more stable and homogenous [35].

The elemental mapping and chemical analysis of the $Fe_{70}Ti_{10}B_{20}$ (at.%) alloys were given in Figure 6. It was seen from Figure that Fe, Ti and B were uniformly distributed in $Fe_{70}Ti_{10}B_{20}$ (at.%) alloy and there were not any contaminations. The results are also in good agreement with the XRD analysis (Figure 3). The EDX analysis also indicated the homogenous chemical composition of alloyed powders and similar atomic compositions of initial powder mixtures were observed.

Figure 7 shows the particle size distributions of the $Fe_{70}Ti_{10}B_{20}$ powders at different milling period. Since

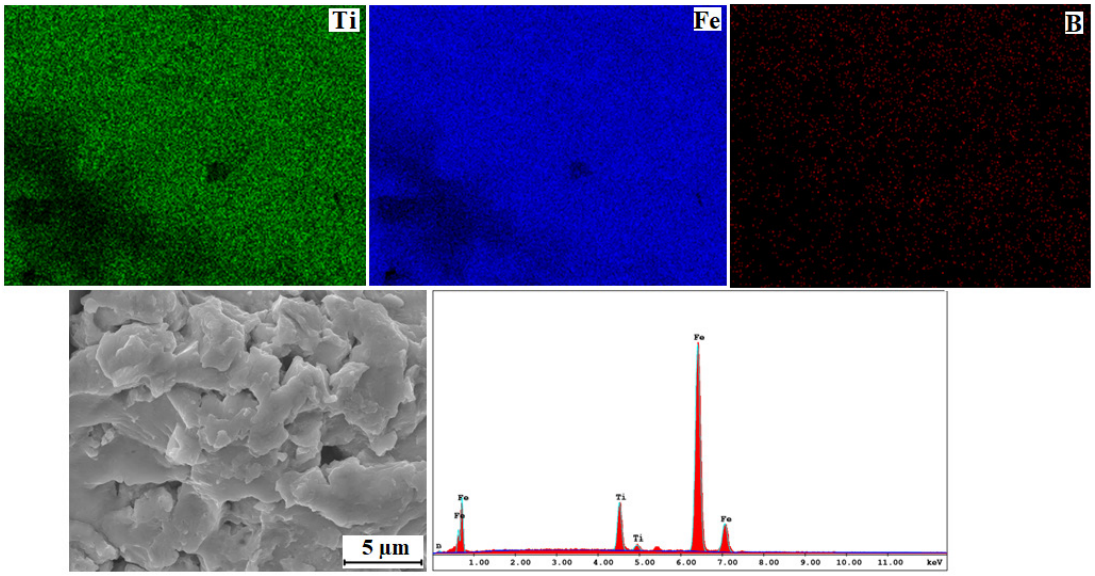

Figure 6. The elemental mapping and EDX analysis of the $Fe_{70}Ti_{10}B_{20}$ (at.%) alloys after 70 h ball milling

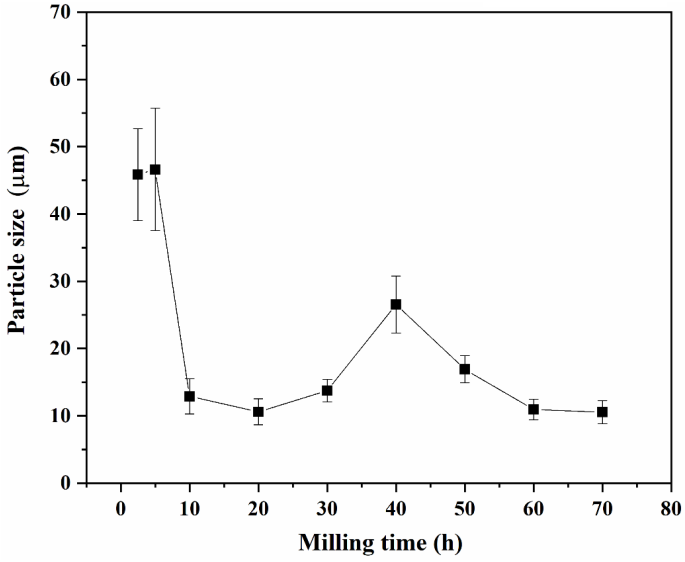

Figure 7. Particle size distributions of MA $Fe_{70}Ti_{10}B_{20}$ powders at different milling period.

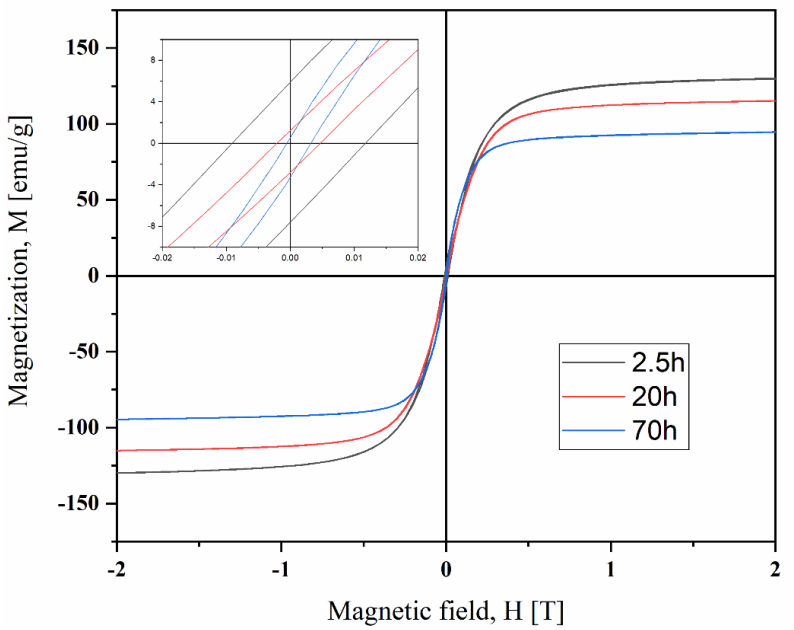

Figure 8. Hysteresis loops of the $Fe_{70}Ti_{10}B_{20}$ (at.%) powders at 300 K

the particles may have composed of several crystallites, particle size is a microscopic phenomenon and mostly greater than the crystallite size [7]. The particulates are composed of many crystallites of varying sizes and orientations and SEM images revealed individual crystallites within the relatively larger powder particles sizes. At the beginning of the milling processes, the particle size increases due to repetitive impacts between vial, balls and powders and leads to an increment of particle sizes. With milling up to 20 h, particles are flattened and fractured and particle size reduces to about 10.6 µm. On continuous milling, the particles were repeated to fracture and cold-weld again so that particles size increases to 26.5µm at 40 h of milling. After this period, particles got work hardened and the overall particle size becomes regular due to balance between welding and fracturing. The similar trends in particle size distribution was also observed in the study of Yousefi et al [18] and Avar [4]. As it is well known, the magnetic properties of the nanostructured materials are substantially different from traditional materials and the magnetic properties are depending on some properties such as chemical content, particle size and morphology etc. of the materials [31]. Hysteresis loops of the $Fe_{70}Ti_{10}B_{20}$ powders (magnetization, M versus to applied magnetic field, H) obtained with 2.5, 20 and 70 h of ball milling samples at 300 K were given in Figure 8. It can be seen from hysteresis curves that all synthesized powders showed the soft ferromagnetic behavior. It was also observed that saturation magnetization (M_s) values decreased due to amorphization and distribution of non-magnetic Ti and B elements in the alloyed powders while coercivity (H_c) values increased due to strain and impurities. The M_s and H_c were found as 130, 110 and 94 emu/g and 32, 47 and 117 (Oe) for 2.5, 20 and 70 h milled powders respectively.

Conclusions

In the present study, $Fe_{70}Ti_{10}B_{20}$ (at.%) alloys were successfully synthesized by elemental Fe, Ti and B powders via planetary type ball mill. The phase, morphological and magnetic properties of powders were investigated by XRD, SEM and VSM method. It is found that firstly Ti and B were dissolved in Fe lattice and Fe-based solid solution formed and then amorphous phases of Fe(TiB) were observed. The crystallite size was decreased to 8.2 nm while lattice strain increased to its maximum value 1.16% after 30 h of milling. SEM images showed the irregular agglomerated form of particles in the range of 10-48 µm. Magnetic analysis at room temperatures revealed the soft magnetic behaviors of mechanical alloyed powders and the saturation magnetization (M_s) and coercivity (H_c) were found as 94 emu/g and 117 Oe, respectively after 70 h of milling.

References

[1] Suryanarayana C., Mechanical alloying and milling, Prog. Mater. Sci., 46, 1–184, 2001.

[2] Avar B., Simsek T., Gogebakan M., Mekanik alaşımlama ile üretilen Nanokristal $Fe_{60}Al_{30}Cu_{10}$ (at.%) tozların yapısal ve mekanik özellikleri, G.U. J. Sci. Part C, 7 (1) 184-191, 2019.

[3] Koch C. C., Cavin O. B., Mckamey C. G., Scarborough J. O., Preparation of “amorphous” $Ni_{60}Nb_{40}$ by mechanical alloying, Appl. Phys. Lett., 43, 1017–1019, 1983.

[4] Avar B., Structural, thermal and magnetic characterization of nanocrystalline $Co_{65}Ti_{25}W_5B_5$ powders prepared by mechanical alloying, J. Non-Cryst. Solids., 432, 246–253, 2016.

[5] Şimşek T., Şimşek T., Ozcan T., Synthesis and characterization of Mn_2B nanocrystals by mechanical alloying method, Boron, 4 , 25-30, 2019.

[6] Birringer R., Nanocrystalline materials, Mater. Sci. Eng. A., 117, 33-43, 1989.

[7] Simsek T., Pure YbB_6 nanocrystals: First time synthesis via mechanochemical method, Adv. Powder Technol., 30, 1219–1225, 2019.

[8] Zawrah M., Shaw L., Microstructure and hardness of nanostructured Al–Fe–Cr–Ti alloys through mechanical alloying, Mater. Sci. Eng. A., 355, 37-49, 2003.

[9] Krifa M., Mhadhbi M., Escoda L., Güell J. M., Sunnol J. J., Isern N. L., Guzmaan C. A., Khitouni M., Nanocrystalline $(Fe_{60}Al_{40})_{80}Cu_{20}$ alloy prepared by mechanical alloying, J. Alloys Compd., 554, 51–58, 2013.

[10] Bahrami A. H., Ghayour H., Sharafi S., Evolution of microstructural and magnetic properties of mechanically alloyed $Fe_{80-x}Ni_{20}Si_x$ nanostructured powders, Powder Technol., 249 7–14, 2013.

[11] Sharifati A., Sharafi S., Structure and magnetic properties of mechanically alloyed $(Fe_{70}Co_{30})_{91}Cu_9$ powder, Mater. Design., 36, 35–40, 2012.

[12] McHenry M. E., Willard M. A., Laughlin D. E., Amorphous and nanocrystalline materials for applications as soft magnets, Prog. Mater. Sci., 44, 291-433, 1999.

[13] Yoshizawa Y., Yamauchi K., Yamane T., Sugihara H., Common mode choke cores using the new Fe based alloys composed of ultrafine grain structure, J. Appl Phys., 64, 6044, 1988.

[14] Shokrollahi H., The magnetic and structural properties of the most important alloys of iron produced by mechanical alloying, Mater. Design., 30, 3374–3387, 2009.

[15] Jiles D., Introduction to Magnetism and Magnetic Materials, Chapman & Hall, London, 280–297, 1991.

[16] Cullity B. D., Graham C. D., Introduction to Magnetic Materials, seconded, Wiley-IEEE Press, New Jersey, 2009.

[17] Baghbaderani H. A., Sharafi S., Chermahini M. D., Investigation of nanostructure formation mechanism and magnetic properties in $Fe_{45}Co_{45}Ni_{10}$ system synthesized by mechanical alloying, Powder Technol., 230, 241–246, 2012.

[18] Yousefi M., Sharafi S., Mehrolhosseiny A., Correlation between structural parameters and magnetic properties of ball milled nano-crystalline Fe–Co–Si powders, Adv. Powder Technol., 25, 752–760, 2014.

[19] Younes A., Dilmi N., Khorchef M., Bouamer A., Bacha N. E., Zergoug M., Structural and magnetic properties of FeCuNi nanostructured produced by mechanical alloying, Appl. Surf. Sci., 446, 258-265, 2018.

[20] Alleg S., Ibrir M., Fenineche N. E., Azzaza S., Bensalem R., Sunol J. J., Magnetic and structural characterization of the mechanically alloyed $Fe_{75}Si_{15}B_{10}$ powders, J. Alloys Compd., 494, 109–11, 2010.

[21] Ipus J. J., Blaazquez J. S., Franco V., Conde A., The use of amorphous boron powder enhances mechanical alloying in soft magnetic FeNbB alloy: A magnetic study, J. Appl Phys., 113-115, 2013.

[22] Okumura H., Ishirara K. N., Shingu P. H., Park H. S., Mechanical alloying of Fe-B alloys, J. Mater. Sci., 27, 153-160, 1992.

[23] Abbasi S., Eslamizadeh H., Raanaei H., Study of synthesis, structural and magnetic properties of nanostructured $(Fe_{67}Ni_{33})_{70}Ti_{10}B_{20}$ alloy, J. Magn. Magn. Mater., 451, 780–786, 2018.

[24] Lashgari H. R., Chu D., Xie S., Sun H., Ferry M., Li S., Composition dependence of the microstructure and soft magnetic properties of Fe-based amorphous/ nanocrystalline alloys: A review study, J. Non-Cryst. Solids., 391, 61–82, 2014.

[25] Lu Z. P., Liu C. T., Thomepson J. R., Porter W. D., Structural Amorphous Steels, Phys. Rev. Lett., 92 (24), 245503, 2004.

[26] Shen J., Chen Q., Sun J., Fan H., Wang G., Exceptionally high glass-forming ability of an FeCoCrMoCBY alloy, Appl. Phys. Lett., 86, 151907, 2005.

[27] El-Eskandarany M. S., Zhang W., Inoue A., Glass-forming ability and magnetic properties of mechanically solid-state reacted $Co_{100-x}Ti_x$ alloy powders, J. Alloys Compd., 350, 232–245, 2003.

[28] Raanaei H., Hosseini V. M., Morphology and magnetic behavior of cobalt rich amorphous/ nanocrystalline $(Co–Ni)_{70}Ti_{10}B_{20}$ alloyed powders, J. Magn. Magn. Mater., 414, 90–96, 2016.

[29] Williamson G. K., Hall W. H., X-ray line broadening from filed aluminium and wolfram, Acta Metall., 1, 22–31, 1953.

[30] Raanaei, H., Fakhraee, M., Synthesis and characterization of nanocrystalline Co-Fe-Nb- Ta-B alloy, J. Magn. Magn. Mater., 438, 144-151, 2017.

[31] Avar B., Nanokristal $Co_{70}Si_{15}B_{15}$ Toz alaşımların yapısal, termal ve manyetik özelliklerinin incelenmesi, SDÜ Fen Bil. Enst. Der., 23, 83-89, 2019.

[32] Karimi L., Shokrollahi H., Structural, microstructural and magnetic properties of amorphous/nanocrystalline $Ni_{63}Fe_{13}Mo_4Nb_{20}$ powders prepared by mechanical alloying, J. Alloys Compd., 509, 6571–6577, 2011.

[33] Koohkan R., Sharafi S., Shokrollahi H., Janghorban K., Preparation of nanocrystalline Fe–Ni powders by mechanical alloying used in soft magnetic composites, J. Magn. Magn. Mater., 320, 1089–1094, 2008.

[34] Khaneghahi S. F., Sharafi S., Magnetic and structural properties of nanostructured $(Fe_{65}Co_{35})_{100-x}Cr_x$ (x = 0, 10) powders prepared by mechanical alloying process, Adv. Powder Technol., 25, 211–218, 2014.

[35] Shokrollahi H., Chermahini M. D., Zandrahimi M., Sharafi S., The effect of milling time and composition on microstructural and magnetic properties of nanostructured Fe–Co alloys, J. Alloys Compd., 477, 45–50, 2009.